Diameter-Dependent Photocurrent in InAsSb Nanowire Infrared Photodetectors.

Svensson, Johannes; Anttu, Nicklas; Vainorius, Neimantas; Borg, Mattias; Wernersson, Lars-Erik

Published in:
Nano Letters

DOI:
10.1021/nl303751d

2013

Diameter Dependent Photocurrent in Infrared InAsSb Nanowire Photodetectors

Johannes Svensson[1,*], Nicklas Anttu[2], Neimantas Vainorius[2], B. Mattias Borg[1,ǂ], Lars-Erik Wernersson[1]

[1]Electrical and Information Technology, Lund University, Box 118, SE-221 00 Lund, Sweden

[2]Solid State Physics, Lund University, Box 118, SE-221 00 Lund, Sweden

[ǂ] Presently at IBM Research – Zürich, CH-8803 Rüschlikon, Switzerland

[*]email: johannes@eit.lth.se

Photoconductors using vertical arrays of InAs/$InAs_{1-x}Sb_x$ nanowires with varying Sb composition *x* have been fabricated and characterized. The spectrally resolved photocurrents are strongly diameter dependent with peaks, which are red-shifted with diameter, appearing for thicker wires. Results from numerical simulations are in good agreement with the experimental data and reveal that the peaks are due resonant modes that enhance the coupling of light into the wires. Through proper selection of wire diameter, the absorptance can be increased by more than one order of magnitude at a specific wavelength compared to a thin planar film with the same amount of material. A maximum 20% cut-off wavelength of 5.7 µm is obtained at 5K for a wire diameter of 717 nm at a Sb content of x = 0.62, but simulations predict that detection at longer wavelengths can be achieved by increasing the diameter. Furthermore, photodetection in InAsSb nanowire arrays integrated on Si substrates is also demonstrated.

Keywords: nanowires, long wavelength infrared, photodetector, InAsSb, resonant absorption

Photodetectors operating in the long-wavelength infrared band (LWIR) (8-14 µm) are important for e.g. thermal imaging of objects at room temperature and gas analysis. There is a large incentive to develop new materials for such detectors due to stability, uniformity and

toxicity issues with commonly used HgCdTe.[1] InAsSb is a suitable choice due to its high thermal conductivity and mobility, weak dependence of band gap on composition and its ability to form useful heterostructures with other III-V semiconductors. The band gap of $InAs_{1-x}Sb_x$ can be tuned by varying the relative composition of As and Sb and reach the narrowest room-temperature band gap of E_g = 100 meV at x = 0.65 corresponding to a wavelength of 12 µm.[2] A photoresponse up to 14 µm have been achieved for x = 0.77 at room temperature illustrating the possibility of LWIR operation.[3] Previous work have mostly focused on $InAs_{1-x}Sb_x$ with $x \approx 0.1$[4-7] or $x > 0.85$[8] since the lattice-mismatch to commercially available GaSb and InSb substrates, respectively, is small and therefore high quality planar layers can be achieved through epitaxial growth. However, to obtain a sufficiently narrow band gap to enable detection in the LWIR band, intermediate chemical compositions are required. If such materials are grown on a binary III-V substrate, the large lattice-mismatch results in strain-relaxation through defect formation.[9] Since such defects act as recombination centres that reduce the carrier lifetime[3, 10], the performance of the detector is severely degraded. In this paper, we present results on InAsSb photodetectors fabricated with an alternative approach to reduce the impact of the lattice-mismatch problem and obtain compositions suitable for detection in the LWIR band. By growing heterostructure InAs/InAsSb nanowires on InAs substrates, the lattice-mismatch problem can effectively be reduced as the strain is released mainly through radial relaxation instead of defect creation.[11, 12] We observe a spectral photocurrent that is strongly dependent on wire diameter and with a peak in the response, which is due to resonant absorption as confirmed through numerical simulations. Recently, diameter dependent peaks in the visible range have been predicted theoretically[13] and also observed in photocurrent[14] and absorption[15] measurements on nanowires, which have major implications for e.g. photovoltaic and

photodetector applications. There are a few previous reports on InAsSb nanowire growth[16-18] but no optoelectronic devices were fabricated using these wires. Previous work on nanowire photodetectors have mostly focused on the visible spectral region[19] with only a few reports on detection of infrared radiation using InAsP nanowires allowing detection up to 1.9 µm at 5 K.[20,21]

Nominally undoped InAs/$InAs_{1-x}Sb_x$ nanowires with x = 0.04 - 0.76 were grown from 50 nm diameter Au particles, deposited on S-doped InAs(111)B substrates with a carrier concentration of 4-8*10^{16} cm^{-3}, using metal-organic vapour phase epitaxy as described in Borg et al.[18] The composition of the $InAs_{1-x}Sb_x$ segments were determined by high resolution X-ray diffraction (XRD) and confirmed on a few compositions by energy dispersive X-ray spectroscopy in a transmission electron microscope. By reducing the density of wires, the effective V/III ratio close to the wires can be increased, resulting in increased radial overgrowth on the InAsSb wire segment[22] allowing us to controllably vary the nanowire diameter (Figure 1a) while keeping the same composition (Figure S1 in supporting information). Due to the random positions of the Au seed particles the diameter distributions of the wires have standard deviations of 3 to 10%. Photodetectors were fabricated by spin coating the substrates with S1800 photoresist that just barely covers the wires. Part of the substrates were cleared from resist and nanowires to enable contact formation to the bottom of the wires before the resist is permanent baked at 200°C for 40 min. Reactive ion etching in oxygen plasma was then used to expose the tip of the wires. A 3 s dip in HCl and rinsing in isopropanol removed the native oxide and subsequent angular thermal evaporation of 10 nm Ti / 500 nm Au through a shadow mask with circular holes

with diameters ranging from 75 to 225 µm resulted in contacts to the tips of the wires and to the substrate (Figure 1b). Electrical and optical characterisation was performed in a Bomem DA8 Fourier transform infrared (FTIR) spectrometer equipped with a liquid-He cryostat. Back-side illumination through the InAs substrate with a globar source was used for optical characterization, since front-side illumination would result in reflection by the thick top contacts. An additional benefit of the backside illumination is that light traverses the wires twice due to the highly reflecting front contact and thus absorption is further increased. The top of the wires were biased and the current from the substrate contact converted to a voltage using a current-to-voltage amplifier with a 100 Hz high-pass filter before the signal was routed into the FTIR spectrometer. At photon energies above the InAs band gap, the substrate acts as a filter blocking the light from reaching the nanowires. All spectral photocurrent measurements were performed at 5 K to reduce the noise imposed by the large dark current at higher temperatures. The spectra were normalized by a reference spectrum obtained by measuring the light transmitted through an InAs substrate using a Deuterated Triglycine Sulfate (DTGS) detector. Figure 1c shows a representative current-voltage characteristic in dark and with all-wavelength IR illumination for approximately 8000 wires with a diameter of d=587±60 nm and x = 0.76. Illumination results in a photocurrent of a few 10's of nA per wire at a bias of 0.25 V (Figure 1c). Spectrally resolved photocurrent measurements of InAs/$InAs_{1-x}Sb_x$ nanowires with d = 75 - 190 nm with varying composition surprisingly reveal that the spectral response depends quite weakly on composition with only a minor increase in wavelength with increasing x (Figure 2a). Also the photocurrent is limited below 4.5 µm even for compositions that should have a sufficiently narrow band gap for detection at longer wavelengths. Note that bolometric effects are found to have a negligible impact on the spectra, since different wavelength modulation speeds give

identical results. In addition, the shapes of the spectra are found to be insensitive to bias and number of wires in a device. In contrast to the results for thin wires, the spectral photocurrent measured on six samples with identical nanowire composition (x = 0.27), but diameters ranging from 269 nm to 661 nm reveal a striking diameter dependence (Figure 2b). As the diameter is increased, a clear peak in the response appears that is shifted towards longer wavelengths. In fact, large diameter wires with d > 500 nm and different composition all exhibit a peak in the spectral photocurrent (Figure 2c). The highest 20% cut-off wavelength of 5.7 μm is obtained for a device with wires with x = 0.62 and d = 717 nm. However, the band gap for x = 0.62 at 5 K corresponds to a wavelength of 9 μm indicating that the cut-off is limited by the diameter and not composition for this device. It is interesting to note that a similar long wavelength cut-off is also observed for a sample where the individual wires are thin but where sample fabrication has led to the agglomeration of wires into thicker bundles (Figure 3). This sample exhibits a broad peak in the photocurrent in spite of the small wire diameter. A small difference in the absorption spectra between 60 and 80 nm diameter InSb nanowires have previously been reported and was attributed to an increase in the band gap due to quantum confinement.[23] However, the wavelength dependence of the photocurrent observed here occurs at diameters significantly larger than the exciton Bohr radius and thus confinement should have negligible effect on the band gap. CuPt ordering, which is known to lower the band gap of InAsSb[24], has previously been observed in the radially grown shell of InAsSb nanowires.[16] However, such band gap lowering effect would be too small to induce the strong diameter dependence observed in the experimental data and does not provide any explanation to the occurrence of the peaks. The large sensitivity of the spectral response to the nanowire diameter is instead attributed to the wavelength and geometry dependent coupling of light into the nanowires.[25] To

investigate this diameter dependence of the absorption in detail, electromagnetic modelling using a scattering matrix method[26, 27] was performed. In the modelling, cylindrical wires of length *L* and with diameter *d* were placed in a square array with pitch *p* and embedded in a dielectric with a refractive index of *n* = 1.6 corresponding to the resist. Light was incident normally from the InAs substrate with a refractive index of *n* = 3.5. If the highly reflecting Au front contact is included, strong interference effects occur (Figure S2 in supporting information). However, such interference effects are not discernible in the measurement results (Figure 2). This discrepancy could be due to the finite distribution of wire diameters and lengths in the experimental devices compared to the arrays with identical wires used in the simulations or due to variations in wire geometry or surface roughness. Therefore, the Au front contact was not included in the modelling and instead the wire length is doubled to account for the round-trip that occurs in the presence of the Au contact in the experimental devices. The optical properties of the wire material are described by the bulk refractive index of InSb[28]. Variations in the absorption coefficient of InAsSb compared to InSb are expected to only affect the magnitude of the absorption but not the shape of the absorption spectra for the studied diameter range. The modelling therefore yields results that can be qualitatively compared to the experimental measurements. To study the diameter dependence of the absorption without effects from a varying amount of absorbing material in the wires, we consider *L* = 6 µm long wires with a fixed diameter to pitch ratio of *d/p*=0.2, corresponding to a 3.1% area coverage. The calculated absorptance at longer wavelengths increases with increasing wire diameter and a peak appears for *d* > 400 nm (Figure 4). The position of this peak, and its red-shift with increasing diameter, are in agreement with the experimental results. However, the experimental spectra exhibit broader peaks than the simulated ones, which can be attributed to the relatively large variation in wire diameter on

a sample. Important to note is that the simulations give a peak position which is insensitive to wire length (Figure S3) and is independent of whether a top tapered part of the wires is included in the modelling (Figure S4). The position of the simulated peak shifts linearly from λ = 3 μm at d = 480 nm to λ = 6 μm at d = 950 nm. For a fixed λ = 4.5 μm the absorptance increases from A = 0.02 to A = 0.60, and then drops to A = 0.10, as the diameter is first increased from d = 200 nm to d = 700 nm and then further to d = 1200 nm. Thus, the absorptance can be increased more than one order of magnitude through a proper selection of wire diameter without increasing the amount of absorbing material. We have found from modelling that it is possible to reach an absorptance of A = 0.60 also with d = 200 nm wires if their length is increased. However, this requires an increase of the length to 300 μm. A striking implication of the absorption peak is that an array with d = 700 nm wires at 3.1% coverage has an absorptance at λ = 4.5 μm, which is more than ten times higher than a planar film (A = 0.05) with the same amount of material. To obtain a peak response at a wavelength corresponding to the band gap of $InAsSb_{0.65}$ at room temperature, extrapolation of the simulation results indicate that the wire diameter needs to be increased to d = 1.6 μm. To elucidate the origin of the absorptance peak, the electric field distribution for λ = 4.5 μm for d = 200, 700, and 1200 nm wires is shown in Figure 5. For d = 700 nm (Figure 5b), that is, at the absorptance peak, we find strong field strengths inside the wire due to the resonant excitation of the HE11 waveguide mode.[13] Both for smaller (Figure 5a) and larger (Figure 5c) diameters, the field strength inside the wires is considerably lower. The source of this resonant excitation of the HE11 mode at d = 700 nm can be qualitatively understood by studying the electric field distribution of the HE11 mode as a function of wire diameter (insets in Figure 5). For d = 200 nm we find that the mode corresponds closely to a plane wave localized to the resist between the wires (inset in Figure 5a). Therefore, for this small

diameter, there is large overlap between the incident plane wave and the HE11 mode, and thus a large fraction of the incident light is coupled to this mode. However, since the field is expelled from the interior of the wires, the mode is absorbed weakly leading to a low absorptance. For d = 1200 nm we notice the opposite behavior where the field of the mode is localized to the interior of the wire (inset in Figure 5c), and thus the mode is absorbed strongly. However, in this case the overlap between the incident plane wave and the field of the mode is small. Thus, only a small fraction of the incident light is coupled to the mode, and the mode contributes only weakly to the absorptance. At the resonant diameter of *d* = 700 nm, the field of the mode shows considerable extension outside the wire as well as a noticeable field strength inside the wire (inset in Figure 5b). Thus, a large fraction of the incident light is coupled to the mode and therefore also into the wire, resulting in the resonant excitation that gives rise to the absorptance peak. A quantitative analysis of the absorption contribution from the HE11 mode is given in the supporting information. A simulation where only the absorptance of the HE11 mode is taken into account (Figure S6) yields an absorptance peak in very good agreement with the peak found in Figure 4b. This agreement corroborates the above assignment of the resonant excitation of the HE11 mode as the origin of the absorptance peak in Figure 4b. In addition to using InAs substrates, devices have also been fabricated using InAs/InAsSb wires grown on undoped Si(111) substrates with a 300 nm Sn-doped InAs layer on top (Figure 2c).[29] Not only does the Si act as a transparent window for incoming light but the demonstrated integration of III-V IR photodetectors on Si is an important step towards low-cost fabrication.

In order for photodetectors using InAsSb wires to be technologically competitive compared to other alternatives, the dark current needs to be reduced substantially to allow for operation at higher temperatures. This can be achieved through the incorporation of

heterostructures with large band gap materials, which act as electron or hole barriers, through axial or radial growth. In summary, we have demonstrated InAsSb nanowire photodetectors with a diameter dependent photocurrent and report the longest cut-off wavelength for any nanowire device reported so far. Simulations revealed that resonant modes in the wires result in strong absorption at a specific wavelength. The diameter of the wires should thus be adjusted by radial growth to obtain peak absorption close to the InAsSb band gap enabling more than one order of magnitude higher absorption than in a corresponding thin film. The results presented here illustrate that InAsSb nanowires are suitable for infrared photodetectors due to the possibility to obtain compositions with a narrow band gap while still maintaining a high crystal quality due to the small InAs/InAsSb heterojunction size and due to their highly efficient absorption at a specific wavelength. These features, in combination with the possibility of Si integration, show great promise for the development of highly competitive infrared photodetectors.

Acknowledgement

This work was supported in part by the Swedish Foundation for Strategic Research (SSF), the Swedish Research Council (VR), the EU program AMON-RA (No. 214814), the Nordic Innovation program NANORDSUN, the E.ON AG as part of the E.ON International Research Initiative, the Nanometer Structure Consortium at Lund University and by the Knut and Alice Wallenberg Foundation.

Supporting information

Figure of XRD data for wires with two different diameters but equal composition and figures that describes the modelling in detail. Section concerning the absorption contribution of the HE11 mode. This material is available free of charge via the Internet at http://pubs.acs.org.

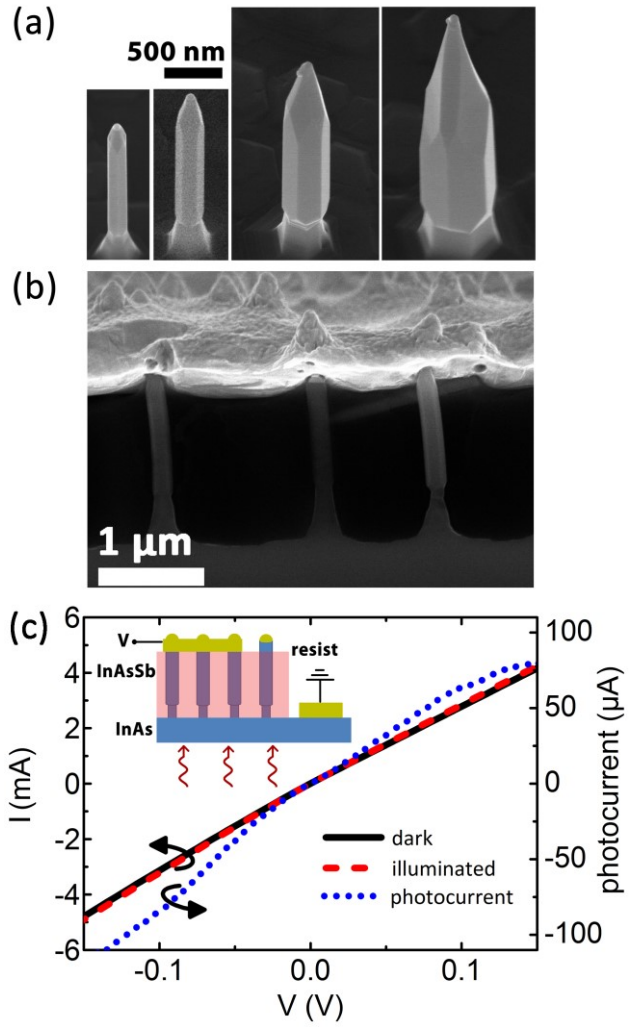

Figure 1. Device illustration and electrical characteristics. (a) SEM images of InAs/$InAs_{1-x}Sb_x$ wires with x = 0.27 from samples with a wire density of 1, 0.5, 0.2 and 0.1 μm^{-2} (left to right) obtained at 30° tilt. (b) Cross sectional SEM image of InAs/$InAs_{1-x}Sb_x$ wires with x = 0.27, a resist spacer and a top Ti/Au contact. (c) Current-Voltage characteristics at 5 K for a device with approximately 8000 InAs/$InAs_{1-x}Sb_x$ wires with x = 0.76, d = 587±60 nm and length of 1.95 µm in dark and with all-wavelength illumination from a globar source. Inset depicts a backside illuminated nanowire array photodetector.

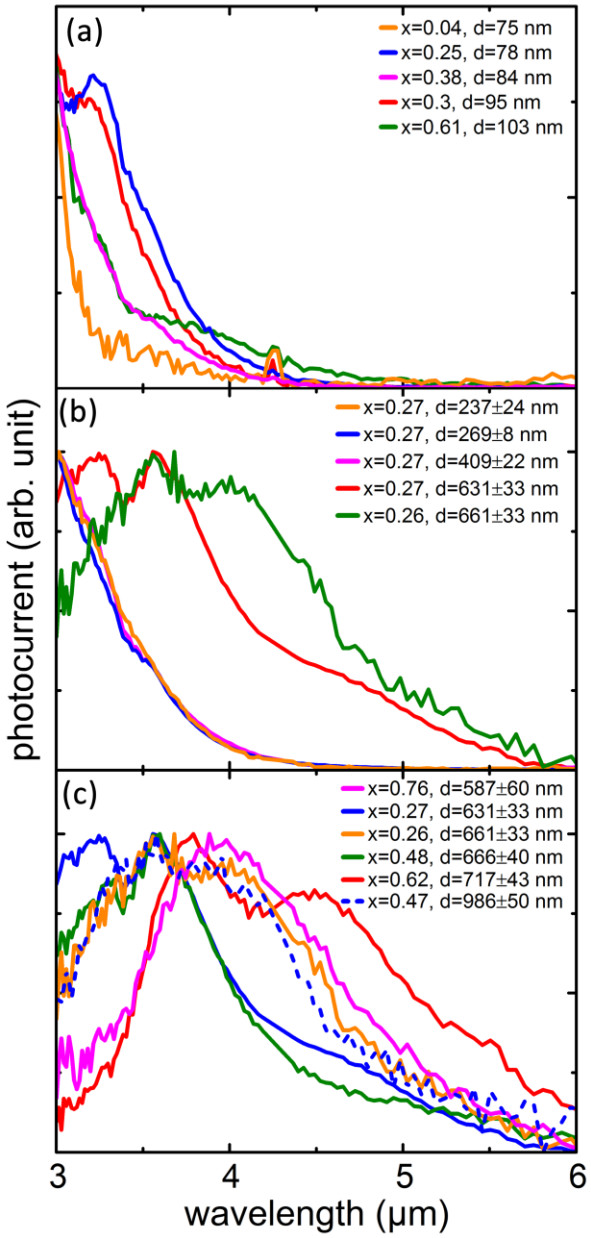

Figure 2. Photocurrent spectra at 5K. The curves have been normalised to the maximum photocurrent. (a) InAs/$InAs_{1-x}Sb_x$ nanowires with different *x* and diameters between 75 and 103 nm at -0.5V bias. (b) Wires of different diameters with *x* = 0.26±0.01 at -0.1 to -0.4 V

bias. (c) Large diameter wires with different *x* at -0.06 to -0.35 V bias. The dashed line corresponds to a device on a Si substrate.

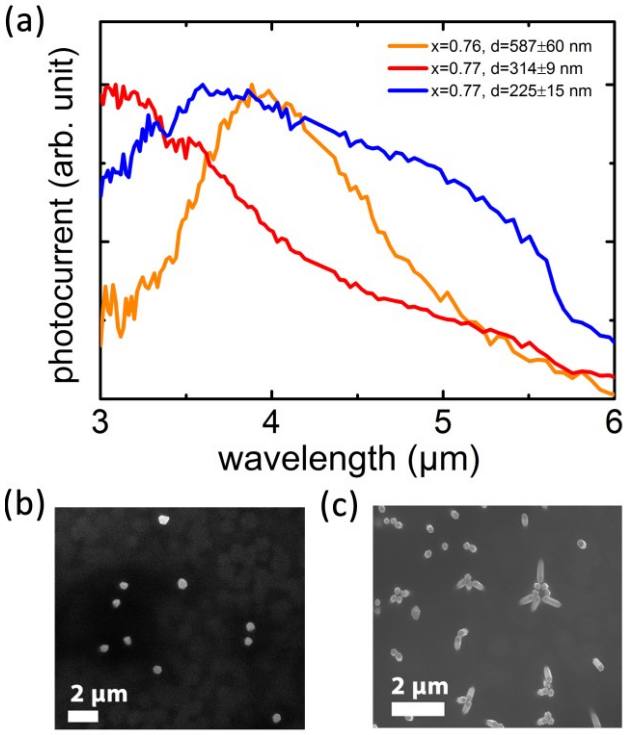

Figure 3. Effect of agglomeration on photocurrent spectra. (a) Photocurrent spectra of InAs/$InAs_{1-x}Sb_x$ nanowires with the same composition *x* = 0.77±1 nm and diameters between 225 and 587 nm. The curves have been normalised to the maximum photocurrent. (b) SEM image of the sample with *d* = 587 nm with separate wires protruding through resist. (c) SEM image of the sample with *d* = 225 nm revealing that many of the wires have agglomerated into bundles. The large variation in bundle size is responsible for the broad photocurrent response.

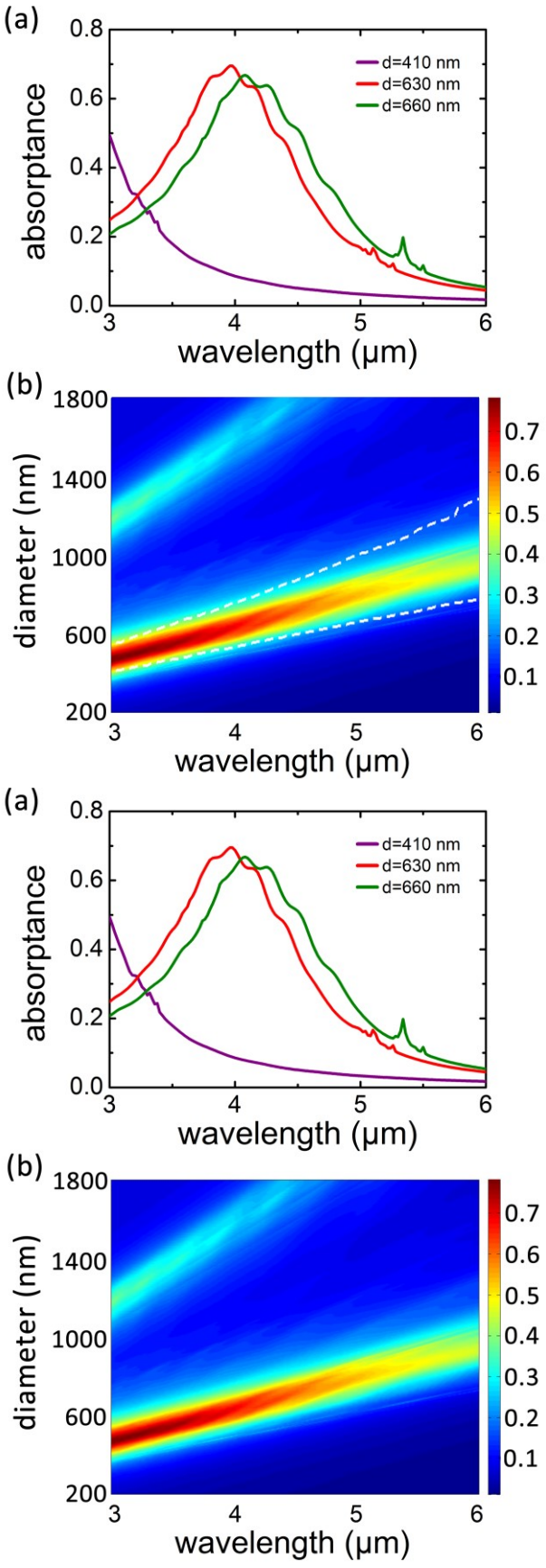
(a)
absorptance
wavelength (μm)
d=410 nm
d=630 nm
d=660 nm
(b)
diameter (nm)
wavelength (μm)
(a)
absorptance
wavelength (μm)
d=410 nm
d=630 nm
d=660 nm
(b)
diameter (nm)
wavelength (μm)

Figure 4. Simulated absorptance for arrays of 6 µm long InSb wires at a constant d/p=0.2. (a) Wires with diameters corresponding to devices in figure 2b. (b) Absorptance as a function of wavelength and wire diameter. A strong absorptance peak red-shifting with diameter is clearly seen as well as a weaker second peak for large diameters. The area enclosed by the dashed lines indicates for which wavelengths and diameters the absorptance is five times higher than in a thin film with the corresponding amount of material.

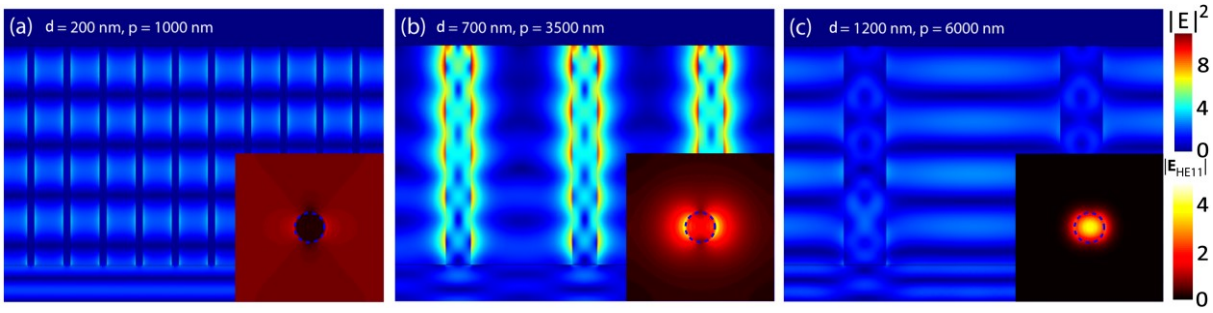

Figure 5. Electric field intensity in 200 nm (a), 700 nm, (b) and 1200 nm (c) diameter InSb wires embedded in a dielectric with n = 1.6 for light of λ = 4.5 µm and an field strength of $|\boldsymbol{E}_{inc}|$=1 normally incident from the bottom InAs substrate with n = 3.5. There is only weak penetration of the electric field into the d = 200 nm wire, leading to a low absorptance of A = 0.02. When the diameter is increased to d = 700 nm, resonant excitation of the HE11 mode occurs, leading to high field intensity inside the wire resulting in an absorptance of A = 0.60. As the diameter is increased to d = 1200 nm, the resonant excitation disappears, the electric field intensity inside the wires drops, and the absorptance decreases to A = 0.10. The insets depict the electric field distribution of the HE11 mode in a single unit cell of the array in top view for the corresponding wires.

1. Rogalski, A. *Prog. Quantum Electron.* **2003,** 27, 59-210.
2. Wieder, H. H.; Clawson, A. R. *Thin Solid Films* **1973,** 15, 217-221.
3. Kim, J. D.; Wu, D.; Wojkowski, J.; Piotrowski, J.; Xu, J.; Razeghi, M. *Appl. Phys. Lett.* **1996,** 68, 99-101.
4. Cheung, D. T.; Andrews, A. M.; Gertner, E. R.; Williams, G. M.; Clarke, J. E.; Pasko, J. G.; Longo, J. T. *Appl. Phys. Lett.* **1977,** 30, 587-589.
5. Carras, M.; Renard, C.; Marcadet, X.; Reverchon, J. L.; Vinter, B.; Berger, V. *Semicond. Sci. Technol.* **2006,** 21, 1720.
6. Sharabani, Y.; Paltiel, Y.; Sher, A.; Raizman, A.; Zussman, A. *Appl. Phys. Lett.* **2007,** 90, 232106.
7. Shao, H.; Li, W.; Torfi, A.; Moscicka, D.; Wang, W. I. *IEEE Photonics Technol. Lett.* **2006,** 18, 1756-1758.
8. Kim, J. D.; Kim, S.; Wu, D.; Wojkowski, J.; Xu, J.; Piotrowski, J.; Bigan, E.; Razeghi, M. *Appl. Phys. Lett.* **1995,** 67, 2645-2647.
9. Chyi, J.-I.; Kalem, S.; Kumar, N. S.; Litton, C. W.; Morkoc, H. *Appl. Phys. Lett.* **1988,** 53, 1092-1094.
10. Rakovska, A.; Berger, V.; Marcadet, X.; Vinter, B.; Bouzehouane, K.; Kaplan, D. *Semicond. Sci. Technol.* **2000,** 15, 34.
11. Caroff, P.; Messing, M. E.; Borg, B. M.; Dick, K. A.; Deppert, K.; Wernersson, L. E. *Nanotechnol.* **2009,** 20, 495606.
12. Ercolani, D.; Rossi, F.; Li, A.; Roddaro, S.; Grillo, V.; Salviati, G.; Beltram, F.; Sorba, L. *Nanotechnol.* **2009,** 20, 505605.
13. Wang, B.; Leu, P. W. *Opt. Lett.* **2012,** 37, 3756-3758.
14. Kim, S.-K.; Day, R. W.; Cahoon, J. F.; Kempa, T. J.; Song, K.-D.; Park, H.-G.; Lieber, C. M. *Nano Lett.* **2012,** 12, 4971-4976.
15. Seo, K.; Wober, M.; Steinvurzel, P.; Schonbrun, E.; Dan, Y.; Ellenbogen, T.; Crozier, K. B. *Nano Lett.* **2011,** 11, 1851-1856.
16. Ercolani, D.; Gemmi, M.; Nasi, L.; Rossi, F.; Pea, M.; Li, A.; Salviati, G.; Beltram, F.; Sorba, L. *Nanotechnol.* **2012,** 23, 115606.
17. Xu, T.; Dick, K. A.; Plissard, S.; Nguyen, T. H.; Makoudi, Y.; Berthe, M.; Nys, J.-P.; Wallart, X.; Grandidier, B.; Caroff, P. *Nanotechnol.* **2012,** 23, 095702.
18. Borg, M. B.; Dick, K. A.; Eymery, J.; Wernersson, L.-E. *Appl. Phys. Lett.* **2011,** 98, 113104.
19. Vj, L.; Oh, J.; Nayak, A. P.; Katzenmeyer, A. M.; Gilchrist, K. H.; Grego, S.; Kobayashi, N. P.; Wang, S. Y.; Talin, A. A.; Dhar, N. K.; Islam, M. S. *IEEE J. Sel. Top. Quantum Electron.* **2011,** 17, 1002-1032.
20. Pettersson, H.; Tragardh, J.; Persson, A. I.; Landin, L.; Hessman, D.; Samuelson, L. *Nano Lett.* **2006,** 6, 229.
21. Tragardh, J.; Persson, A. I.; Wagner, J. B.; Hessman, D.; Samuelson, L. *Jour. Appl. Phys.* **2007,** 101, 123701.
22. Plissard, S. R.; Slapak, D. R.; Verheijen, M. A.; Hocevar, M.; Immink, G. W. G.; van Weperen, I.; Nadj-Perge, S.; Frolov, S. M.; Kouwenhoven, L. P.; Bakkers, E. P. A. M. *Nano Lett.* **2012,** 12, 1794-1798.
23. Yang, Y.; Li, L.; Huang, X.; Li, G.; Zhang, L. *J. Mater. Sci.* **2007,** 42, 2753-2757.
24. Kurtz, S. R.; Dawson, L. R.; Biefeld, R. M.; Follstaedt, D. M.; Doyle, B. L. *Phys. Rev. B* **1992,** 46, 1909-1912.
25. Wu, P. M.; Anttu, N.; Xu, H. Q.; Samuelson, L.; Pistol, M.-E. *Nano Lett.* **2012,** 12, 1990-1995.
26. Anttu, N.; Xu, H. Q. *J. Nanosci. Nanotechnol.* **2010,** 10, 7183-7187.
27. Anttu, N.; Xu, H. Q. *Physical Review B* **2011,** 83, 165431.
28. Holm, R. T., Indium Antimonide (InSb). In *Handbook of Optical Constants of Solids*, Academic Press: Burlington, **1997**, 491-502.

29. Gorji Ghalamestani, S.; Berg, M.; Dick, K. A.; Wernersson, L.-E. *J. Cryst. Growth* **2011,** 332, 12-16.